





A Binocular Vision SSVEP Brain–Computer Interface Paradigm for Dual-Frequency Modulation

Yike Sun , Graduate Student Member, IEEE, Liyan Liang, Jingnan Sun, Xiaogang Chen , Member, IEEE, Runfa Tian, Yuanfang Chen , Lijian Zhang, and Xiaorong Gao 

Abstract—Objective: This study presents a novel brain-computer interface paradigm of dual-frequency modulated steady-state visual evoked potential (SSVEP), aiming to suppress the unpredictable intermodulation components in current applications. This paradigm is especially suitable for training-free scenarios. **Approach:** This study built a dual-frequency binocular vision SSVEP brain-computer interface system using circularly polarized light technology. Two experiments, including a 6-target offline experiment and a 40-target online experiment, were taken with this system. Meanwhile, an improved algorithm filter bank dual-frequency canonical correlation analysis (FBDFCCA) was presented for the dual-frequency SSVEP paradigm. **Main results:** Energy analysis was conducted for 9 subjects in the 6-target dual-frequency offline experiment, among which the signal-to-noise ratio of target frequency components have increased by 2 dB compared to the one of unpredictable intermodulation components. Subsequently, the online experiment with 40 targets was conducted with 12 subjects. With this new dual-frequency paradigm, the online training-free experiment's average information transmission rate (ITR) reached 104.56 ± 15.74 bits/min, which was almost twice as fast as the current best dual-frequency paradigm. And the average information transfer rate for offline training analysis of this new paradigm was 180.87 ± 17.88 bits/min. **Significance:** These results demonstrate

that this new dual-frequency SSVEP brain-computer interface paradigm can suppress the unpredictable intermodulation harmonics and generate higher quality responses while completing dual-frequency encoding. Moreover, its performance shows high ITR in applications both with and without training. It is thus believed that this paradigm is competent for achieving large target numbers in brain-computer interface systems and has more possible practices.

Index Terms—Brain-computer interface, steady-state visual evoked potentials, binocular vision, dual-frequency modulation, polarized light.

I. INTRODUCTION

STEADY-state visual evoked potentials (SSVEPs) are natural response of the optical nervous system. When people fixate on a periodically flickering stimulus target, the visual cortex of the brain generates responses and harmonics with corresponding frequencies [1]. Because its response is stable and can be directly measured by electroencephalography (EEG), SSVEPs have been widely used among brain-computer interface systems [2], [3]. Since the SSVEP based brain-computer interface paradigm has apparent advantages in information transmission rate and training time [4], it has been one of the hottest research areas of the brain-computer interface in recent decades [5].

Light waves are transverse waves, and their direction of vibration and propagation form a plane of vibration. If the plane is fixed, the light is linearly polarized [6]. Two sets of orthogonal linear polarized light can create elliptically polarized light. Suppose the amplitudes of two sets light are equal. In that case, it is called circularly polarized light, and the angle between two groups of linearly polarized light is the phase of circularly polarized light [7]. Glasses made with circularly polarized light plates can only pass through the circularly polarized light of the target phase, enabling both eyes to receive different pictures simultaneously [8]. The stereo vision scheme of circularly polarized light has a better viewing angle and light intensity than linear polarization [9].

At present, the SSVEP brain-computer interface primarily uses single-frequency targets for stimuli, and the most typical choice is the 40-target stimulus model [10]. Currently, there are two principal algorithms for the single-frequency model: the training-free algorithm and the training algorithm [11].

Manuscript received 5 November 2021; revised 20 February 2022 and 17 August 2022; accepted 2 October 2022. Date of publication 5 October 2022; date of current version 21 March 2023. This work was supported in part by the Key Research and Development Program of Ningxia, under Grant 2022CMG02026, in part by the National Natural Science Foundation of China, under Grant 62171473, and in part by the Tianjin Municipal Science and Technology Plan Project under Grant 21JC YBJC01500. (Corresponding author: Xiaorong Gao.)

Yike Sun and Jingnan Sun are with the Department of Biomedical Engineering, Tsinghua University, China.

Liyan Liang is with the China Academy of Information and Communications Technology, China.

Xiaogang Chen is with the Institute of Biomedical Engineering, Chinese Academy of Medical Sciences and Peking Union Medical College, China.

Runfa Tian is with the Department of Neurosurgery, Beijing Tiantan Hospital and Beijing Key Laboratory of Central Nervous System Injury, Beijing Neurosurgical Institute, Capital Medical University, China.

Yuanfang Chen and Lijian Zhang are with the Beijing Institute of Mechanical Equipment, China.

Xiaorong Gao is with the Department of Biomedical Engineering, Tsinghua University, Beijing 100084, China (e-mail: gxr-dea@mail.tsinghua.edu.cn).

Digital Object Identifier 10.1109/TBME.2022.3212192

The representative algorithm without training algorithm is filter bank canonical correlation analysis (FBCCA) [12], proposed by Chen et al. in 2015, and the usual algorithm with training is task-related component analysis (TRCA) [13], [14]. Both algorithms can achieve very high information transfer rates in practice [11]. Nevertheless, because the optimal response frequency band of SSVEP is relatively fixed [1], when the number of targets increases, the stimulus frequency spacing decreases. Dual-frequency stimuli can code C_n^2 stimulus targets using n different frequencies. Therefore, it is necessary to develop a dual-frequency stimulus paradigm to accommodate future scenarios with numerous targets. In recent years, some researchers have proposed several methods for dual-frequency stimuli, which can be roughly divided into two modes: the checkerboard arrangement paradigm [15] and the left-right field of view paradigm [16]. The checkerboard arrangement paradigm [17] improved by Liang et al. in 2020 is the most stable dual-frequency SSVEP paradigm.

However, the current methods cannot avoid unpredictable intermodulation harmonic components, which form can be expressed as $a * f_1 + b * f_2$ (a and b can be arbitrary integers because of the huge individual differences [15], [16], [17], [18], [19]), so it is challenging to realize a training-free application [17]. Some studies have used these harmonic components for coding, but the effect is insignificant because those harmonics are unstable, and individual differences are significant [18], [19]. Therefore, finding a method to suppress or avoid aliasing frequency is of great significance for developing the dual-frequency SSVEP paradigm.

Early in 1996, some scholars found that the frequency that stimulates both eyes can reduce the generation of intermodulation frequencies [20]. In order to solve the above problem, this study proposes a new design solution of dual-frequency SSVEP paradigm with binocular separation, which uses circularly polarized light modulation to isolate both eyes to suppress the generation of $a * f_1 + b * f_2$ form of the unpredictable intermodulation harmonic components. Based on filter bank canonical correlation analysis (FBCCA), this paper also proposes filter bank dual-frequency canonical correlation analysis (FBDCCA) dedicated to the dual-frequency SSVEP paradigm. First, the offline experiment of 6 targets is carried out, and a variety of signal-to-noise ratios are compared with the classical dual-frequency paradigm checkerboard arrangement [15], [17]. Second, the algorithm FBDCCA is used to measure 40 targets online training-free experiments to compare the ITR and accuracy of the binocular vision and checkerboard arrangement paradigms. The collected data are used to compare offline with the TRCA training-based algorithm.

II. METHODS

A. Binocular Vision Dual-Frequency SSVEP Paradigm

To solve the problems of unstable responses induced by the dual-frequency paradigm and susceptibility to generate unpredictable intermodulation components, this study proposed a way to stabilize the induced response by using circularly polarized

light to achieve binocular separation. Its core method architecture is shown in Fig. 1. Currently, circularly polarized light displays on the market can simultaneously transmit two different pictures with polarized light of different phases in the form of alternating odd and even rows [21].

As shown in Fig. 1(a), the polarization screen transmits two stimulation frequencies simultaneously. Because the height of each row is minimal, the stimulus can be approximately the sum of the two signals for human eyes. When subjects do not wear polarization glasses or use other polarization demodulation equipment, they will receive two overlapping stimulation frequency pictures. After passing through polarization glasses or using other polarization demodulation equipment, the original overlapping picture is divided into two independent stimulation frequency images. These two frequency signals will subsequently be independently assigned to the visual cortex along with the visual pathways of both eyes. Through this polarized light system, we successfully generated a binocular vision stimulation at the same position, at the same time but with different frequencies for the left and right eyes of the subjects. Fig. 1(b) shows the physical picture.

The signal received by most mammals' left and right eyes is in the form of dominant ocular columns alternately distributed over areas of the visual cortex, with the source of the signal changing every 0.5-mm from one eye [22]. Therefore, binocular separation is designed to guarantee that the signals received by both eyes will be mixed and more evenly received at the visual cortex (in subjects without tremendous amplitude binocular laterality), as shown in Fig. 1(a). The binocular split vision design guarantees that the signals received by both eyes do not overlap before the optic chiasm, instead of overlapping at the level of the retina, helping to reduce the unpredictable intermodulation harmonic frequencies.

B. Design of Experiments

This study was divided into two main experiments. Experiment 1 compared the binocular vision paradigm with the checkerboard arrangement paradigm in terms of signal-to-noise ratio. An offline crossover experiment with 6 targets was conducted to verify the stability of the binocular vision paradigm in terms of evoked potential energy. Experiment 2 aimed to compare the performance of the two paradigms, and an online no-training crossover experiment with 40 targets was conducted. The data were analyzed offline for training to verify the superiority of the binocular vision paradigm in practical applications. The frequency phase encoding of the stimulus targets was selected using the encoding method that Liang et al. used [17] in Experiment 1 and Experiment 2.

The diagram of a single target for the binocular vision and checkerboard arrangement paradigms is shown in Fig. 2. Fig. 2(a) is a diagram of a single target in the binocular vision paradigm. A stimulus square alternates two frequencies in odd and even rows on a polarized display, each row being 1 pixel high. Each target stimulus square is 132×132 pixels in size. Fig. 2(b) is a single-target schematic diagram of the checkerboard arrangement paradigm designed by Liang et al. in

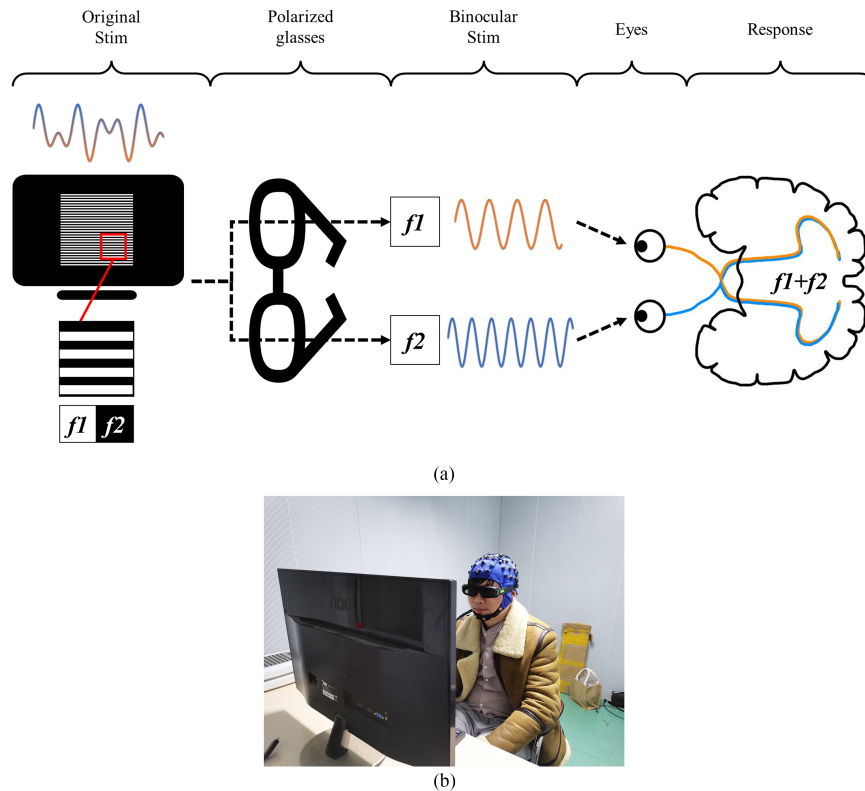


Fig. 1. (a) Schematic diagram of the working principle of the binocular vision paradigm system with a polarization display. Mixed frequency is emitted with polarized light at two angles synchronously and then demodulated into two stimulation frequencies by polarization glasses. The two subsequent stimulus frequencies are assigned to two eyes and reach the visual cortex along the visual transmission pathway. (b) Physical photos of the binocular vision paradigm system.

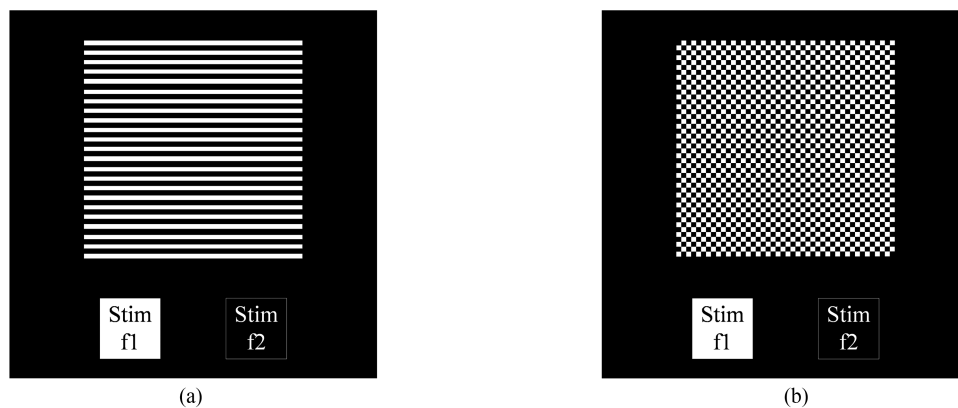


Fig. 2. (a) Binocular vision SSVEP paradigm single target schematic. Alternating odd and even rows show two frequencies, each row being 1 pixel high. Each target stimulus square is 132×132 pixels in size. (b) Checkerboard arrangement of the dual-frequency SSVEP paradigm single target schematic; each target has a total of 44×44 small squares. Each target stimulus square is 132×132 pixels in size.

2020 [17]. Each target has 44×44 small squares, each of which is 3×3 pixels in size, and the total size of a single stimulus target is 132×132 pixels. In a multi-target experiment, each stimulus target is evenly distributed on a screen of 1920×1080 pixels.

1) Experiment 1: Offline SNR Analysis Experiment: Experiment 1 was a 6-target offline experiment designed to compare the signal-to-noise ratio of evoked potentials between the binocular vision paradigm and the traditional checkerboard arrangement paradigm. The coding scheme was shown in Fig. 3(a) according to Liang et al. in 2020 [17]. The stimulation

frequency and phase of each target were: $[9, 13.8 \text{ Hz}|0\pi]$, $[9, 16.2 \text{ Hz}|0.5\pi]$, $[9.8, 13 \text{ Hz}|0.5\pi]$, $[9.8, 16.2 \text{ Hz}|1\pi]$, $[11.4, 13 \text{ Hz}|0\pi]$, $[12.2, 15.4 \text{ Hz}|0\pi]$.

For the convenience of calculating the amplitude spectrum, the duration of stimulation was determined as 5 seconds. A single trial diagram is shown in Fig. 3(b), in which each trial began with a 1-second cue and then followed by a 5-second stimulation period, and a 2-second black screen inter trial interval. There were 30 trials in each group of blocks, with five attempts per stimulation target, and the stimulation sequence was randomly

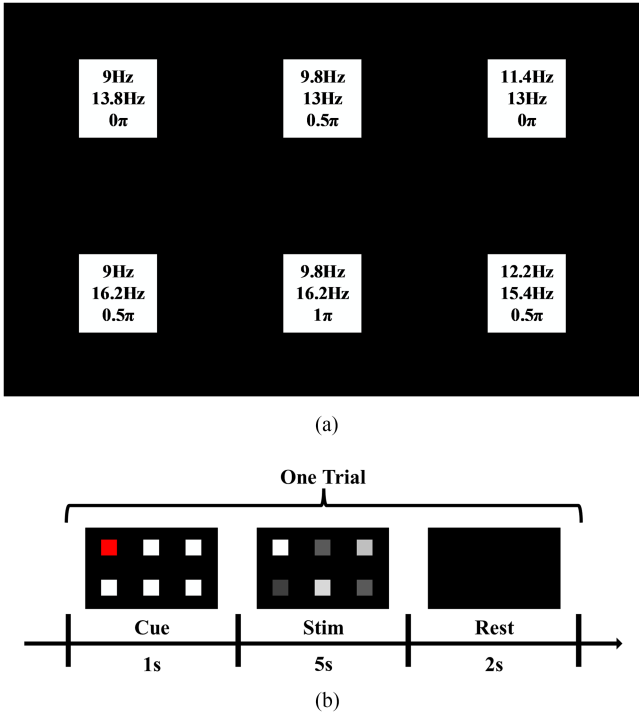


Fig. 3. (a) Schematic diagram of Experiment 1 coding and stimulation. (b) Schematic diagram of the Experiment 1 single-trial process.

generated. For a single participant, one block was required for each of the two paradigms. There were 2 blocks for each participant in total. The order of block and trial is randomly generated by the computer.

2) Experiment 2: Online BCI Experiment: Experiment 2 was a 40-target and training-free online experiment that compared the ITR and classification accuracy of evoked potentials between binocular vision and traditional checkerboard arrangement paradigms. As shown in Fig. 4(a), frequency and phase coding used the scheme proposed by Liang et al. [17].

A simulation time length of 2 seconds was chosen to test and compare the two paradigms' practical applicability. A single trial diagram was shown in Fig. 4(b), in which each trial began with a 1-second cue and then entered a 2-second stimulation period, followed by a 1-second black screen for rest at the end of the stimulation. Afterward, online feedback was shown on the screen for 1 s, and there was another 1-second black screen rest. There were 40 trials in each group of blocks, one for each stimulation target. For each subject, there were ten blocks in Experiment 2. After one block experiment, the experimental paradigm is switched between binocular vision and checkerboard arrangement, and the next block experiment is conducted based on the paradigm switched. A computer program randomly generated the stimulus order of block and trial under the above rules.

3) Information of Participants: The participants' details can be found in Table I. There were 9 participants in Experiment 1. Four of them were males, aged between 18 and 25 (22 years old on average); five were females, aged between 22 and 25 (23.4 years old on average). The overall average age in Experiment 1

TABLE I
PARTICIPANT INFORMATION STATISTICS

Experiment	Number of subjects	Number of males	Number of females	Mean age
Experiment 1	9	4	5	22.78
Experiment 2	12	5	7	22.17

was 22.78 years old. There were 12 participants in Experiment 2; five were males, aged between 18 and 28 (22.6 years on average); seven were females, ranging from 19 to 25 years old (21.86 years old on average). The overall mean age in Experiment 2 was 22.17 years old.

Subjects 1 and 7 participated in Experiment 1 and Experiment 2 simultaneously, and their numbers in the two experiments were the same. The other subjects only participated in one experiment. All subjects were at least 18 years old citizens of the People's Republic of China. Before the experiment, all subjects were informed about the entire content of the experimental procedure; all had normal vision and no history of photosensitive seizures. Before the experiments, each participant was asked to read and sign the informed consent form approved by the research ethics committee of Tsinghua University. None of the subjects had ever participated in experiments with dual-frequency SSVEP paradigm brain-computer interface systems.

C. Data Acquisition

In this study, the electroencephalographic device of the Synamp2 system (Neuroscan, Inc.) was used. Because this study only separated the two stimuli without introducing other information such as spatial location, it had little effect on the response area of SSVEPs. The nine occipital conductors (Pz, PO5, PO3, POz, PO4, PO6, O1, Oz, O2) were recorded at a sampling rate of 1000 Hz. All electrodes were located following the International 10–20 EEG System. The reference electrode is overhead at the CZ position in the 10–20 EEG system. The ground electrode is located on the forehead. The stimulation screen used an AOC circularly polarized 3D display (D2769Vh, 27 inches, 1920 × 1080) and its associated circularly polarized lens glasses. The simulation program was written using MATLAB 2021a and the Psychophysics Toolbox Version 3 toolbox [23]. Before each experiment begins, each stimulus frame was timed to determine the stability of the visual stimulus generated by the LCD screen. All experiments were conducted in a dark, quiet and shielded electromagnetic environment, while the distance between the subject and the display screen was strictly set as approximately 80 cm.

D. Data Analysis

1) Data Preprocessing: All the experimental data were extracted according to the events triggered by the stimulus program through the parallel port, including data from nine leads. In Experiment 2, the initial 140 ms data were removed according to previous reports [10]. A band-pass IIR ellipse filter (order:30, sections:15, sampling frequency: 1000 Hz, pass-band cutoff frequency: 5 Hz, stop-band cutoff frequency: 100 Hz) was

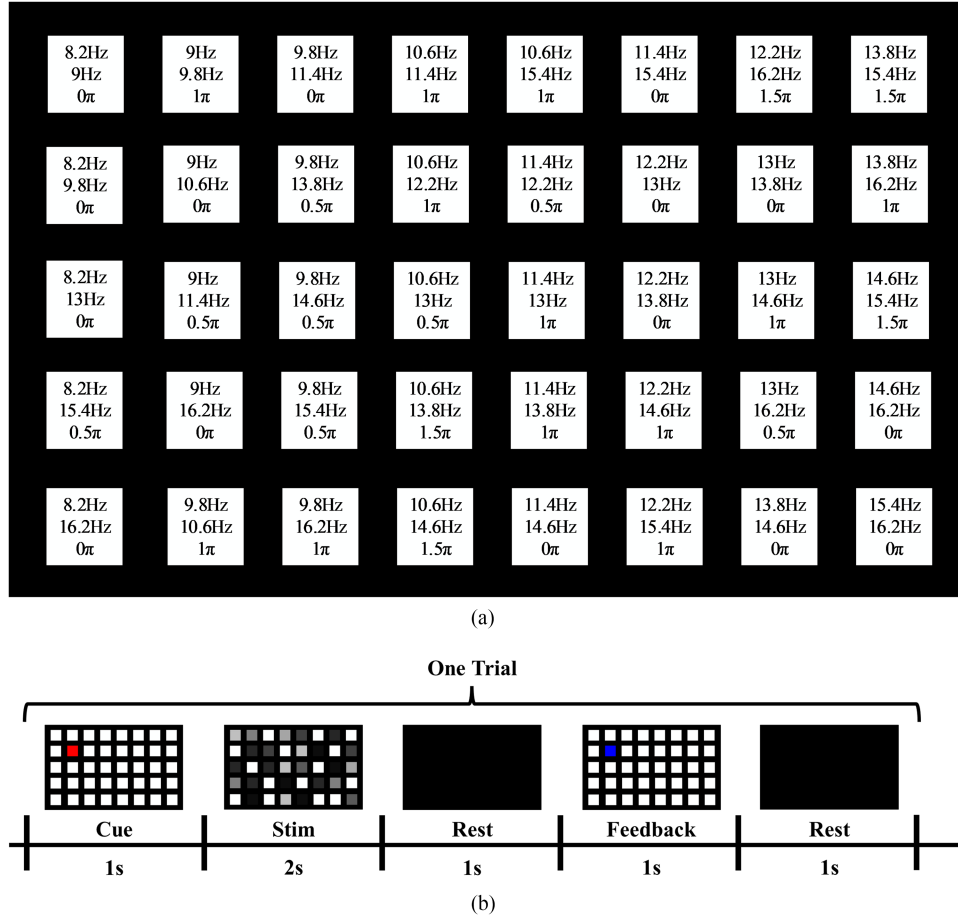


Fig. 4. (a) Schematic diagram of Experiment 2 coding and stimulation. (b) Schematic diagram of the Experiment 2 single-trial process.

used to filter the data, and then the sample was downsampled to 250 Hz for further analysis.

2) Signal-to-Noise Ratio Analysis: The signal-to-noise ratio (SNR) analysis in this study was divided into three parts: broadband SNR, narrowband SNR, and intermodulation SNR.

The broadband SNR is a standard index to measure the quality of VEP signal in electrophysiology, which can comprehensively measure the intensity of the evoked signal [24]. The two frequencies of the dual-frequency code and their 1 to 5 times harmonics were taken as signals, and the remaining frequencies from 5 Hz to 100 Hz are noise, which can be expressed as follows:

$$\text{SNR}_{\text{Broadband}} = \frac{\sum_{\delta=1}^5 [N(\delta f_1) + N(\delta f_2)]}{\sum_{f=5\text{Hz}}^{100\text{Hz}} N(f) - \sum_{\delta=1}^5 [N(\delta f_1) + N(\delta f_2)]} \quad (1)$$

$\text{SNR}_{\text{Broadband}}$ represents the broadband signal-to-noise ratio, $N(f)$ represents the power value of the signal at frequency f , and f_1 and f_2 represent two frequencies of the stimulus target.

Because of the small target frequency interval in the SSVEP paradigm, its signal-to-noise ratio with surrounding frequencies is closely related to its classification performance. So Narrow-band SNR is also a fundamental index for SSVEP brain-computer system [12]. It takes two frequencies and their harmonics from 1 to 5 times as signals. Noise is the other frequencies component in the 2 Hz band centered on each signal. The expressions are as shown in (2), at the bottom of the page.

$\text{SNR}_{\text{Narrowband}}$ denotes the narrowband signal-to-noise ratio, $N(f)$ represents the power value of the signal on frequency f , and f_1 and f_2 denote two frequencies of the stimulus target. Δf is the reciprocal of the sampling time length t of the signal, which can be described as:

$$\Delta f = \frac{1}{t} \quad (3)$$

The intermodulation SNR is an index proposed in this paper to measure the unpredictable intermodulation harmonic component interference of the dual-frequency SSVEP paradigm. We

$$\text{SNR}_{\text{Narrowband}} = \frac{\sum_{\delta=1}^5 [N(\delta f_1) + N(\delta f_2)]}{\sum_{k=-1/\Delta f}^{1/\Delta f} \sum_{\delta=1}^5 [N(k\delta f_1 \Delta f) + N(k\delta f_2 \Delta f)] - \sum_{\delta=1}^5 [N(\delta f_1) + N(\delta f_2)]} \quad (2)$$

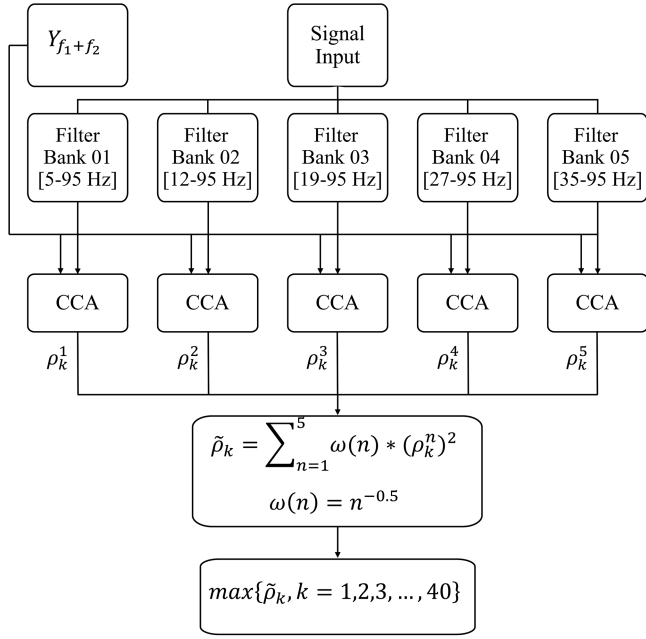


Fig. 5. Schematic diagram of FBDDCA algorithm and parameters used in this study.

consider the two frequencies of the dual-frequency and their harmonics from 1 to 5 times as signals. View the intermodulation harmonics like $a * f_1 + b * f_2$ as noise (take a, b as an integer, and $a, b \in [-5, 5]$). The expression is as follows:

$$\text{SNR}_{\text{Intermodulation}} = \frac{\sum_{\delta=1}^5 [N(\delta f_1) + N(\delta f_2)]}{\sum_{a=-5}^5 \sum_{b=-5}^5 N(a f_1 + b f_2) - \sum_{\delta=1}^5 [N(\delta f_1) + N(\delta f_2)]} \quad (4)$$

$\text{SNR}_{\text{Intermodulation}}$ represents the intermodulation signal-to-noise ratio, $N(f)$ represents the power value of the signal at frequency f , and f_1 and f_2 represent two frequencies of the stimulus target. a and b are integers, where $a, b \in [-5, 5]$.

3) Online Training-Free Analysis With the Filter Bank Dual-Frequency Canonical Correlation Analysis (FBDDCA) Method: Filter bank canonical correlation analysis (FBCCA) is one of the most popular and effective untrained algorithms for SSVEP brain-computer interface [12], but it is unsuitable for the dual-frequency paradigm. Considering there is no mature and reliable untrained recognition algorithm for dual-frequency SSVEPs to date, this paper proposes filter bank dual-frequency canonical correlation analysis (FBDDCA) based on FBCCA. The algorithm's core is to assume that the SSVEP induction process is a non-linear system that satisfies the overlap but not the homogeneity. Considering that the evoked signal is treated as $\text{Response}(f)$, where f is the stimulus frequency. Then the signal evoked by the dual-frequency paradigm is $\text{Response}(f_1 + f_2)$, which the following formulas can represent:

$$\text{Response}(f_1 + f_2) = \lambda_1 * \text{Response}(f_1) + \lambda_2 * \text{Response}(f_2) \quad (5)$$

Where λ_1, λ_2 are the parameters resulting from different propagation paths and different distributions of dominant ocular columns two eyes of a person. For basic FBCCA, the template for the CCA section is as follows:

$$Y_f = \begin{bmatrix} \sin(2\pi f t) \\ \cos(2\pi f t) \\ \vdots \\ \vdots \\ \sin(2\pi N_h f t) \\ \cos(2\pi N_h f t) \end{bmatrix} \quad (6)$$

Y_f is the template for the CCA part of the basic FBCCA, f is the target stimulation frequency, and N_h is the harmonic number, generally set to 5. For the dual-frequency SSVEP paradigm, if the response is $\lambda_1 * \text{Response}(f_1) + \lambda_2 * \text{Response}(f_2)$, we can change the template for the CCA part to:

$$Y_{f_1+f_2} = \begin{bmatrix} \sin(2\pi f_1 t) \\ \cos(2\pi f_1 t) \\ \sin(2\pi f_2 t) \\ \cos(2\pi f_2 t) \\ \vdots \\ \vdots \\ \sin(2\pi N_h f_1 t) \\ \cos(2\pi N_h f_1 t) \\ \sin(2\pi N_h f_2 t) \\ \cos(2\pi N_h f_2 t) \end{bmatrix} \quad (7)$$

$Y_{f_1+f_2}$ is the template of CCA in FBDDCA, f_1, f_2 is the target stimulation frequency, N_h is the number of harmonics used, and 5 is chosen according to reported literature [10]. Experiment 2 in this study has verified that FBDDCA has a good effect on the dual-frequency paradigm. The filter parameters and weight values selected in this paper can be seen in Fig. 5. The filter bank adopted Chebyshev II IIR filter with order of 78.

4) Offline Training Analysis With the Task-Related Component Analysis (TRCA) Method: Task-related component analysis (TRCA) is a widely recognized classical SSVEP training algorithm [13], [14]. With the proposed SSVEP paradigm of joint frequency phase stimulation, effectively utilizing the phase information of SSVEP becomes essential. Nevertheless, classical algorithms such as CCA do not take the phase information into account. TRCA can extract task-related components by maximizing data reproducibility, making full use of the phase information of SSVEP signals. However, it also needs training data as support to represent reality.

In Experiment 2, there were five blocks of data for each paradigm. We used the leave-one-out cross-validation strategy for TRCA training, leaving one block as the test set at a time, and the other four blocks as the training set, training five times in total. The final result is the average of the accuracy rates of the five models. The details of the TRCA algorithm can be found in Nakanishi et al. 2018 [14].

5) Information Transmission Rate (ITR): ITR (in bits/min) has always been an important index to measure the performance of brain-computer interface systems [25]. The calculation formula of the information transmission rate in this paper is as

follows:

$$ITR = \frac{60}{T+0.5} \left\{ \log_2 N + P \log_2 P + (1-P) \log_2 \left[\frac{1-P}{N-1} \right] \right\} \quad (8)$$

Where T is the time length. N is the number of stimuli targets. P is the classification accuracy, and the value is between 0 and 1. Due to the difference between the experiment and the practical use scenario, in order to estimate the actual ITR, we used the selected stimulate time window length in seconds plus the gaze shifting time 0.5s [10] as T .

III. RESULTS

A. Results of Experiment 1: Offline SNR Analysis Experiment

We first calculated the power spectrum obtained by averaging each stimulus target on nine channels in this experiment. The power spectrum obtained by the Oz lead of Subject 07 after averaging the five trials on stimulus target 1 (coded as [9, 13.8 Hz| 0π]) is shown in Fig. 6(a), where Fig. 6(a) is the result of the checkerboard arrangement paradigm. Compared with the binocular vision paradigm, the result of the checkerboard arrangement paradigm clearly shows very significant intermodulation harmonic signals at 22.8 Hz (9 Hz+13.8 Hz) and 9.6 Hz ($-2 * 9$ Hz+ $2 * 13.8$ Hz).

The Experiment 1 signal-to-noise ratio analysis results are shown in Fig. 7, where from left to right are the results of broadband signal-to-noise ratio analysis, narrowband signal-to-noise ratio analysis and intermodulation signal-to-noise ratio analysis.

The result of broadband signal-noise ratio from the binocular vision paradigm ($M = -8.32$ dB, $SD = 2.51$) and the checkerboard arrangement paradigm ($M = -9.5$ dB, $SD = 2.76$) indicate that the binocular vision paradigm significantly improves evoked potentials, $t(8) = 4.47$, $p = .0021 < .01$.

Meanwhile, the binocular vision paradigm narrowband signal-noise ratio ($M = -7.07$ dB, $SD = 2.47$) is also significant higher than the checkerboard arrangement paradigm ($M = -8.31$ dB, $SD = 2.67$), $t(8) = 5.11$, $p = .00091 < .001$.

And the results of average intermodulation signal-noise ratio shows that there is a significant increase in the binocular vision paradigm ($M = 0.95$ dB, $SD = 2.12$) to the checkerboard arrangement paradigm ($M = -1.05$ dB, $SD = 2.34$), $t(8) = 7.98$, $p = .000044 < .001$. Which has increased for 2 dB.

The above data are sufficient to demonstrate that the signal quality induced by the binocular vision paradigm is higher than that of the checkerboard arrangement paradigm. At the same time, we can see that the binocular vision paradigm has significantly fewer intermodulation harmonics than those induced by the board placement paradigm, which further indicates that it is feasible to design an offline training-free system using the binocular vision paradigm.

B. Results of Experiment 2: Online BCI Experiment

Table II shows the online training-free experimental results of experiment 2, using the FBCCA algorithm. The average accuracy of the binocular vision paradigm ($M = 89.83\%$, SD

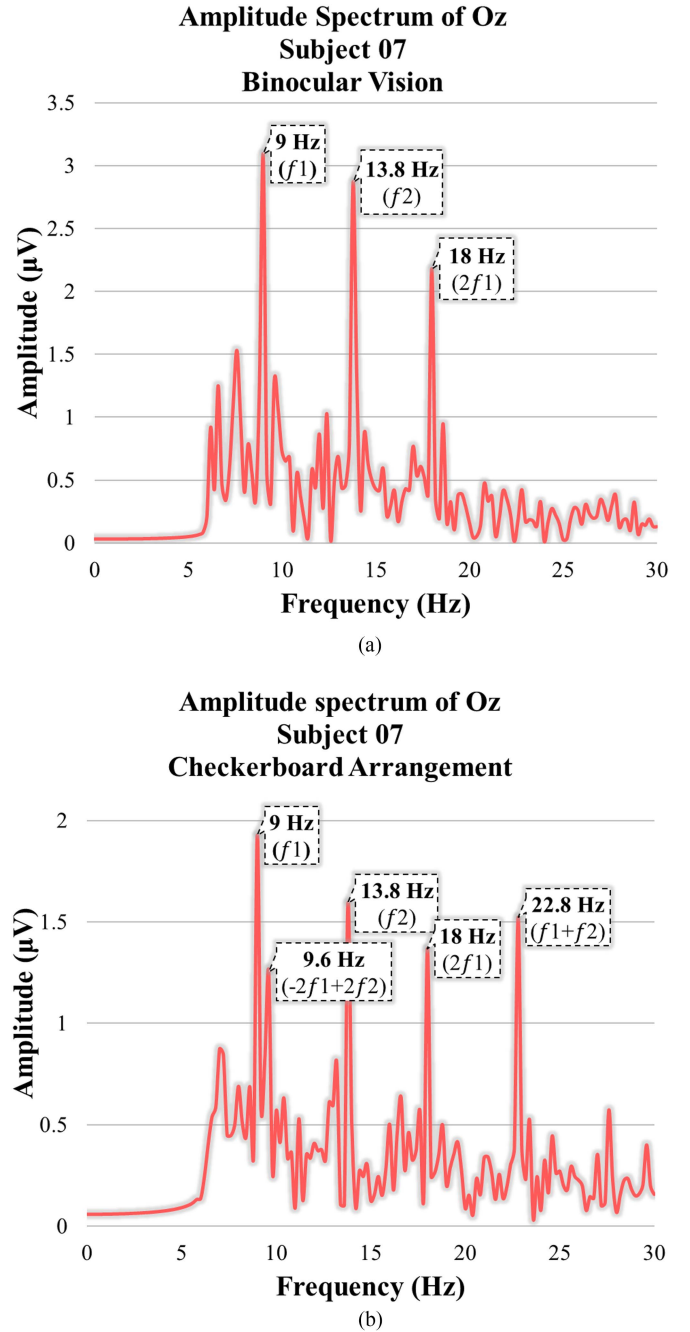


Fig. 6. Experiment 1 Target 1 Power Spectrum (coded as [9, 13.8 Hz| 0π]). (a) Power spectrum of the binocular vision paradigm. (b) Power spectrum of the checkerboard arrangement paradigm.

$= 7.86$) has a significant increase comparing to the checkerboard arrangement paradigm ($M = 57.21\%$, $SD = 19.92$), $t(11) = 5.95$, $p = .000097 < .001$. Meanwhile, there is also a significant increase in the average ITR from the binocular vision paradigm ($M = 104.56$ bits/min, $SD = 15.74$) to the checkerboard arrangement paradigm ($M = 52.57$ bits/min, $SD = 27.63$), $t(11) = 6.89$, $p = .000026 < .001$. In the binocular vision paradigm experiment, 83% of the subjects had accuracy of 85% or more, and 50% had accuracy of 90% or more. In the checkerboard arrangement paradigm experiment, only 17% of the subjects

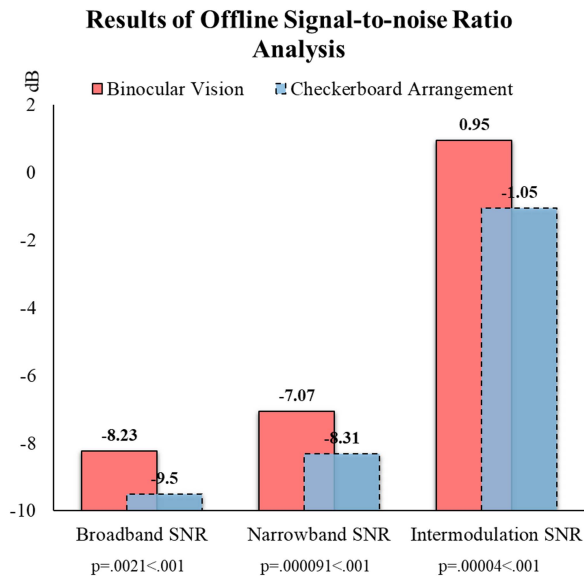


Fig. 7. The broadband, narrowband and intermodulation mean signal-noise ratio results and standard deviation of 9 subjects in Experiment 1.

TABLE II
FBDCCA ONLINE ANALYSIS RESULTS OF EXPERIMENT 2
(TIME LENGTH: 2 S)

Subject Num	ACC(%) of Binocular Vision	Expected ITR(bits/min) of Binocular Vision	ACC(%) of Checkerboard Arrangement	Expected ITR(bits/min) of Checkerboard Arrangement
01	96.5	118.03	61.0	55.10
02	98.0	121.79	87.0	97.86
03	90.0	103.79	67.5	64.67
04	93.0	110.06	25.0	13.12
05	77.0	79.88	37.0	24.99
06	88.0	99.80	53.0	44.17
07	85.5	95.00	63.5	58.70
08	88.5	100.78	64.0	59.44
09	89.5	102.78	60.5	54.39
10	98.5	123.13	29.5	17.30
11	98.5	123.13	88.5	100.78
12	75.0	76.54	50.0	40.30
MEAN±STD	89.83±7.86	104.56±15.74	57.21±19.92	52.57±27.63

achieved an accuracy of more than 85%, and 42% had accuracy of less than 60%.

Fig. 8 shows the offline processing results of the data recorded in experiment 2. When the data length is longer than 0.6 seconds, the ITR and classification accuracy of the binocular vision paradigm is slightly higher than that of the checkerboard arrangement paradigm, but there is no statistical significance.

From the above results, it is not difficult to observe that the binocular vision paradigm has significant advantages over the checkerboard arrangement paradigm under the non-training condition. Moreover, compared with the training-free situation, the ITR and accuracy of the binocular vision paradigm and the checkerboard arrangement paradigm are very similar under training conditions.

Those above results show that while the binocular vision paradigm leads a lot in the training-free situation, it also could

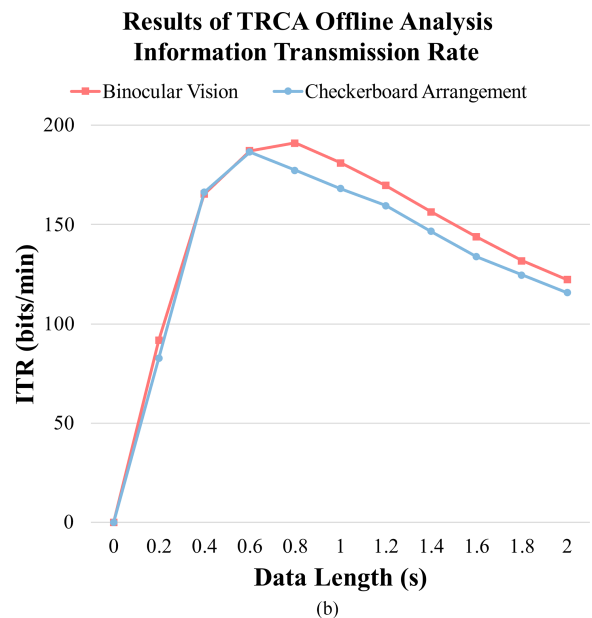
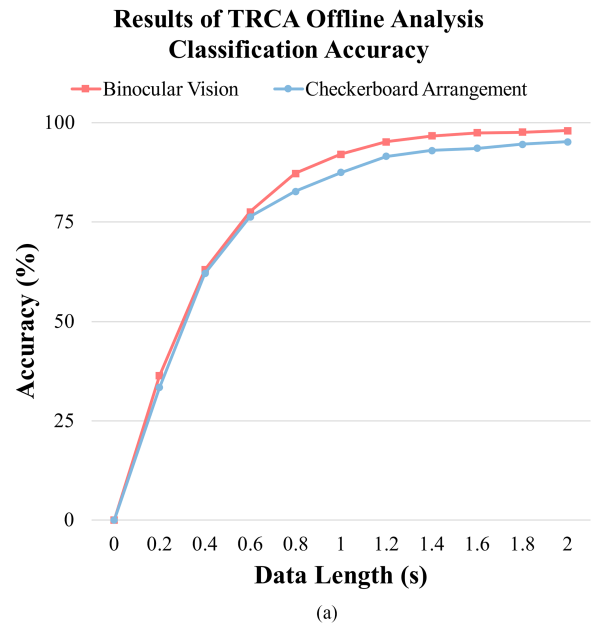


Fig. 8. Results of TRCA offline analysis. (a) Is a diagram showing how the classification accuracy varies with the length of the data. (b) Shows the trend of ITR with the length of data.

achieve high ITR and accuracy with training, which can be easily observed in Fig. 9. For easier comparison, data points with and without training are used when the time window length is 2 seconds.

IV. DISCUSSION

A. Generation of the Unpredictable Intermodulation Harmonics

The binocular vision paradigm can improve the signal-to-noise ratio and reduce, but unfortunately not eradicate, the generation of unpredictable intermodulation harmonics. We believe

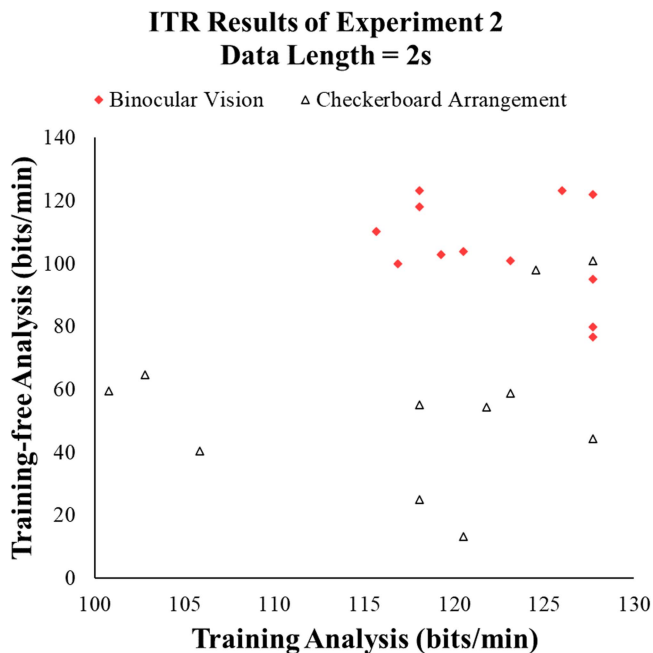


Fig. 9. Scatterplots of training-free and training analysis. Red diamond dots are the results of the binocular vision paradigm. Triangle points of the black outline are the results of the checkerboard arrangement paradigm.

that the source of those frequencies in our paradigm is different from typical dual-frequency paradigms. In terms of the checkerboard arrangement paradigm, the primary source should be the interaction between the peripheral and central visual fields, a phenomenon which is known as surround suppression [26]. When the same eye receives different frequency stimuli at different spatial locations, differences in the central and peripheral visual fields necessarily occur, and their interaction cannot be avoided. Surround suppression is generated in the retina, LGN, as well as the visual cortex [26]. If we consider the response process of SSVEP as a multilevel communication system, surround suppression will introduce noise at almost every layer of the system, resulting in a large number of unpredictable intermodulation frequencies. Whereas for the binocular vision paradigm, the source should be the interaction between the two eyes [28], [29], which occurs mainly in the visual cortex, and no phenomenon is evident in the LGN [30]. In contrast to the checkerboard arrangement paradigm, the surround suppression does not occur when using the binocular vision paradigm where both eyes receive only a single stimulus frequency. Thus, the intermodulation noises which were introduced in layers before the preoptic cortex, such as the retina, are significantly reduced, leading to remarkable improvement in the intermodulation SNR and ITR for BCI system.

B. Other Implementations of Binocular Vision

Polarized glasses on the market cannot completely filter the visual stimulation from the opposite side. During the experiments, it is reported that the subjects can still see the weak contralateral visual stimulation, which will cause a significant

impact on the brain-computer interface system. Given the fact that polarized light technology is more easily affected by external light sources, a much stricter experiment setting is required. The environment should avoid as much light as possible and the sitting posture of subjects are of more demands than the traditional single-frequency SSVEP brain-computer interface paradigm. In summary, further research needs to explore a more reliable and stable way to realize the binocular vision.

Apart from the polarized light form used in this paper, anaglyph 3D and shutter 3D are binocular split vision 3D technologies widely used. Moreover, the technical maturity also fully supports the development of the dual-frequency paradigm of binocular split vision SSVEP [31], [32]. However, these two technologies also have their problems. The red and blue color difference brought by anaglyph 3D and the flicker brought by SSVEPs will be uncomfortable, which may cause epilepsy [33]. In essence, shutter 3D is time-division multiplexing, and the eyes will not receive the stimulation image for half the time [34]. Moreover, due to the high refresh rate, it also has strong need for equipment performance.

C. Further Research & Application of the Binocular Vision Dual-Frequency SSVEP Paradigm

The current research on dual-frequency SSVEP are still dealing with the unpredictable intermodulation harmonics induced by dual-frequency stimulation. The main idea of this paper is to treat the intermodulation components as noise and suppress it by binocular vision, and good results were obtained. Exploring other ways that can also inhibit the generation of the unpredictable intermodulation harmonics will continually be the main direction of our research in the future.

As a dual-frequency SSVEP paradigm, the main application of the binocular vision paradigm lies in the application of large target number coding SSVEP. In this paper, only 11 stimulation frequencies are used to realize the 40-target paradigm, which shows the great potential of this paradigm in large target SSVEP designs. Secondly, the binocular vision paradigm helps understand the binocular rivalry effect. In fact, SSVEPs have been used for a long time to study binocular rivalry [28], [35], [36], [37]. As a low-cost and high reusability SSVEP brain-computer interface paradigm, our presented diagram has a bright and widely applicable future in cognitive research.

V. CONCLUSION

In this paper, we first put forward the design idea of the dual-frequency SSVEP paradigm with binocular separation to suppress the unpredictable intermodulation harmonics. Then we have implemented this paradigm by circular polarized light technique. For application, we have also proposed an improved algorithm FBDCCA on basis of FBCCA to more fit the training-free dual-frequency SSVEP paradigm.

Two experiments were performed in order to verify the performance of the paradigm and the algorithm. Experiment 1 was designed for offline energy analysis. The results shown that this novel paradigm was more significant in signal quality and suppression of aliasing frequency than the classical dual-frequency

paradigm checkerboard arrangement paradigm. Experiment 2 was designed for online training-free validation of paradigm performance, using the algorithm for the FBDCCA proposed above. The mean ITR in the binocular vision paradigm was 104.56 ± 15.74 bits/min, which is 51.99 bits/min higher than the checkerboard arrangement paradigm. The experimental results strongly suggested that the binocular vision paradigm can be used in the dual-frequency SSVEP training-free system. Then, using the data recorded in experiment 2, we did an offline training analysis based on the TRCA algorithm. Although there is no statistical significance, the highest average ITR of the binocular vision paradigm has reached 191.38 ± 30.1 bits/min, slightly higher than that of the checkerboard arrangement paradigm, 177.47 ± 48.98 bits/min, when data length is 0.8 s. It can be noticed that the training results of the binocular vision paradigm were also excellent.

Overall, the dual-frequency SSVEP paradigm can greatly expand the encoding space of the stimulation targets, which would benefit the design of SSVEP-BCI systems with a large number of targets. Furthermore, the binocular vision dual-frequency SSVEP-BCI paradigm also possesses evident advantages in signal quality and intermodulation harmonics suppression. Its recognition performance without training is another non-neglectable strength over other existing dual-frequency paradigms.

ACKNOWLEDGMENT

The authors would like to thank Anruo Shen for English proofreading.

REFERENCES

- [1] N. Galloway, "Human brain electrophysiology: Evoked potentials and evoked magnetic fields in science and medicine," *Brit. J. Ophthalmol.*, vol. 74, no. 4, 1990, Art. no. 255.
- [2] Y. Wang et al., "Brain-computer interfaces based on visual evoked potentials," *IEEE Eng. Med. Biol. Mag.*, vol. 27, no. 5, pp. 64–71, Sep./Oct. 2008, doi: [10.1109/memb.2008.923958](https://doi.org/10.1109/memb.2008.923958).
- [3] X. Gao et al., "Interface, interaction, and intelligence in generalized brain-computer interfaces," *Trends Cogn. Sci.*, vol. 25, no. 8, pp. 671–684, 2021.
- [4] S. Gao et al., "Visual and auditory brain-computer interfaces," *IEEE Trans. Biomed. Eng.*, vol. 61, no. 5, pp. 1436–1447, May 2014, doi: [10.1109/tbme.2014.2300164](https://doi.org/10.1109/tbme.2014.2300164).
- [5] H.-J. Hwang et al., "EEG-based brain-computer interfaces: A thorough literature survey," *Int. J. Hum. Comput. Interact.*, vol. 29, no. 12, pp. 814–826, 2013, doi: [10.1080/10447318.2013.780869](https://doi.org/10.1080/10447318.2013.780869).
- [6] D. S. Kliger and J. W. Lewis, *Polarized Light in Optics and Spectroscopy*. New York, NY, USA: Elsevier, 2012.
- [7] Y. Lu, "Study on the Design and Application of Polarization Imaging Optical System," Ph.D. dissertation, Changchun Inst. Opt., Fine Mechanics Phys., Univ. Chin. Acad. Sci., Changchun, China, 2020.
- [8] Z. Datai, "Research on 3D display technology and its application in education," Master Thesis, Shaanxi Normal Univ., Xi'an, China, 2011.
- [9] N. Kim et al., "3D display technology," *Disp. Imag.*, vol. 1, no. 1, pp. 73–95, 2014.
- [10] X. Chen et al., "High-speed spelling with a noninvasive brain-computer interface," *Proc. Nat. Acad. Sci.*, vol. 112, no. 44, pp. E6058–E6067, 2015, doi: [10.1073/pnas.1508080112](https://doi.org/10.1073/pnas.1508080112).
- [11] R. Zerafa et al., "To train or not to train? A survey on training of feature extraction methods for SSVEP-based BCIs," *J. Neural Eng.*, vol. 15, no. 5, Oct. 2018, Art. no. 051001, doi: [10.1088/1741-2552/aaca6e](https://doi.org/10.1088/1741-2552/aaca6e).
- [12] X. Chen et al., "Filter bank canonical correlation analysis for implementing a high-speed SSVEP-based brain-computer interface," *J. Neural Eng.*, vol. 12, no. 4, 2015, Art. no. 046008.
- [13] Y. Kimura et al., "SSVEP-based brain-computer interfaces using FSK-Modulated visual stimuli," *IEEE Trans. Biomed. Eng.*, vol. 60, no. 10, pp. 2831–2838, Oct. 2013, doi: [10.1109/tbme.2013.2265260](https://doi.org/10.1109/tbme.2013.2265260).
- [14] M. Nakanishi et al., "Enhancing detection of SSVEPs for a high-speed brain speller using task-related component analysis," *IEEE Trans. Biomed. Eng.*, vol. 65, no. 1, pp. 104–112, Jan. 2018, doi: [10.1109/tbme.2017.2694818](https://doi.org/10.1109/tbme.2017.2694818).
- [15] H.-J. Hwang et al., "A new dual-frequency stimulation method to increase the number of visual stimuli for multi-class SSVEP-based brain-computer interface (BCI)," *Brain Res.*, vol. 1515, pp. 66–77, 2013, doi: [10.1016/j.brainres.2013.03.050](https://doi.org/10.1016/j.brainres.2013.03.050).
- [16] Z. Yan et al., "Right-and-left visual field stimulation: A frequency and space mixed coding method for SSVEP based brain-computer interface," *Sci. China Inf. Sci.*, vol. 54, no. 12, pp. 2492–2498, 2011, doi: [10.1007/s11432-011-4503-5](https://doi.org/10.1007/s11432-011-4503-5).
- [17] L. Liang et al., "Optimizing a dual-frequency and phase modulation method for SSVEP-based BCIs," *J. Neural Eng.*, vol. 17, no. 4, Aug. 2020, Art. no. 046026, doi: [10.1088/1741-2552/abaa9b](https://doi.org/10.1088/1741-2552/abaa9b).
- [18] A. Materka and M. Byczuk, "Alternate half-field stimulation technique for SSVEP-based brain-computer interfaces," *Electron. Lett.*, vol. 42, no. 6, pp. 321–322, Mar. 2006, doi: [10.1049/el:20060171](https://doi.org/10.1049/el:20060171).
- [19] K.-K. Shyu et al., "Dual-frequency steady-state visual evoked potential for brain computer interface," *Neurosci. Lett.*, vol. 483, no. 1, pp. 28–31, 2010, doi: [10.1016/j.neulet.2010.07.043](https://doi.org/10.1016/j.neulet.2010.07.043).
- [20] S. Suter et al., "Differentiation of VEP intermodulation and second harmonic components by dichoptic, monocular, and binocular stimulation," *Vis. Neurosci.*, vol. 13, no. 6, pp. 1157–1166, 1996, doi: [10.1017/s0952523800007793](https://doi.org/10.1017/s0952523800007793).
- [21] S. A. Boothroyd, "Projection display systems," U.S. Patent Appl. US8388138B1, 2013.
- [22] J. C. Horton and E. T. Hedley-Whyte, "Mapping of cytochrome oxidase patches and ocular dominance columns in human visual cortex," *Philos. Trans. Roy. Soc. London. B., Biol. Sci.*, vol. 304, no. 1119, pp. 255–272, 1984, doi: [10.1098/rstb.1984.0022](https://doi.org/10.1098/rstb.1984.0022).
- [23] D. H. Brainard and S. Vision, "The psychophysics toolbox," *Spatial Vis.*, vol. 10, no. 4, pp. 433–436, 1997.
- [24] J. Thielen et al., "Broad-band visually evoked potentials: Re (con) volution in brain-computer interfacing," *PLoS one*, vol. 10, no. 7, 2015, Art. no. e0133797.
- [25] D. J. McFarland et al., "BCI signal processing: Feature translation," in *Brain-Computer Interfaces: Principles and Practice*, vol. 8. Oxford, U.K.: Oxford Univ. Press, 2012, pp. 147–165.
- [26] H. Jones et al., "Surround suppression in primate V1," *J. Neurophysiol.*, vol. 86, no. 4, pp. 2011–2028, 2001.
- [27] T. G. Fisher et al., "Retinal and nonretinal contributions to extraclassical surround suppression in the lateral geniculate nucleus," *J. Neurosci.*, vol. 37, no. 1, pp. 226–235, 2017, doi: [10.1523/jneurosci.1577-16.2016](https://doi.org/10.1523/jneurosci.1577-16.2016).
- [28] C. Hou et al., "Contrast normalization accounts for binocular interactions in human striate and extra-striate visual cortex," *J. Neurosci.*, vol. 40, no. 13, pp. 2753–2763, 2020, doi: [10.1523/jneurosci.2043-19.2020](https://doi.org/10.1523/jneurosci.2043-19.2020).
- [29] S. Katyal et al., "Neurons that detect interocular conflict during binocular rivalry revealed with EEG," *J. Vis.*, vol. 16, no. 3, p. 18, 2016, doi: [10.1167/16.3.18](https://doi.org/10.1167/16.3.18).
- [30] S. R. Lehky and J. H. Maunsell, "No binocular rivalry in the LGN of alert macaque monkeys," *Vis. Res.*, vol. 36, no. 9, pp. 1225–1234, 1996.
- [31] A. J. Woods and C. R. Harris, "Comparing levels of crosstalk with red/cyan, blue/yellow, and green/magenta anaglyph 3D glasses," *Proc. SPIE*, 2010, vol. 7524, Art. no. 75240Q.
- [32] H. Wu et al., "Evaluating stereoacuity with 3D shutter glasses technology," *BMC Ophthalmol.*, vol. 16, no. 1, pp. 1–8, 2016.
- [33] R. S. Fisher et al., "Photoc-and pattern-induced seizures: A review for the epilepsy foundation of America working group," *Epilepsia*, vol. 46, no. 9, pp. 1426–1441, 2005.
- [34] H. S. Ko et al., "Display device with 3D shutter control unit," U.S. Patent Appl. US8310527B2, 2012.
- [35] R. Wang et al., "Frequency selection for SSVEP-based binocular rivalry," in *Proc. Conf. 2nd Int. IEEE EMBS Conf. Neural Eng.*, 2005, pp. 600–603.
- [36] K. W. Jamison et al., "SSVEP signatures of binocular rivalry during simultaneous EEG and fMRI," *J. Neurosci. Methods*, vol. 243, pp. 53–62, 2015.
- [37] P. Zhang et al., "Binocular rivalry requires visual attention," *Neuron*, vol. 71, no. 2, pp. 362–369, 2011, doi: [10.1016/j.neuron.2011.05.035](https://doi.org/10.1016/j.neuron.2011.05.035).